Light- and Elevated-Temperature-Induced Degradation-Affected Silicon Cells From a Utility-Scale Photovoltaic System Characterized by Deep-Level Transient Spectroscopy

Steve Johnston , Chuanxiao Xiao, Michael G. Deceglie , Ashley Gaulding , Chun-Sheng Jiang , Harvey Guthrey , Dana B. Kern, George F. Kroeger, Mowafak Al-Jassim, and Ingrid L. Repins

Abstract—Photovoltaic modules from a utility-scale field experienced power loss by light- and elevated-temperature-induced degradation (LeTID). Samples from the affected monocrystalline silicon cells are cored and extracted from the module packaging and then laser-scribed to form 2-mm diameter isolated areas. Using deep-level transient spectroscopy, a majority-carrier, hole-trap defect with an activation energy of 0.42 eV is detected on degraded and regenerated samples. The LeTID-degraded sample, however, has a larger signal corresponding to a trap density of 1.1×10^{13} cm^{-3}, which is about five times larger than the 2.1×10^{12} cm^{-3} trap density of the regenerated sample. An increase in filling pulse time from 50 μs to 20 ms shows a slight decrease in activation energy from 0.42 to 0.36 eV suggesting that the defect level may consist of a band of energy states where shallower states continue to fill with long filling times. The capture rate of the defect is directly measured using an increasing series of filling pulsewidths in 15 to 125 ns range. This leads to a measured capture cross section of 5.1×10^{-17} cm^2, and using an approximate defect density of 10^{13} cm^{-3}, the majority-carrier-hole lifetime related to this defect is approximately 100 μs when in the LeTID-degraded state.

Index Terms—Charge carrier lifetime, degradation, laser ablation, photovoltaic cells, semiconductor impurities, solar panels.

I. Introduction

LIGHT- and elevated-temperature-induced degradation, or LeTID, has been an observed degradation mechanism in multicrystalline and monocrystalline silicon solar cells since 2012 [1], [2]. When detected, this form of degradation has typically led to losses of roughly 3% to 10%, as summarized in the referenced review article [2]. LeTID has been shown to be distinct from boron–oxygen light-induced degradation, and while evidence suggests the mechanism involves hydrogen, much is still unknown about the composition, formation, and regeneration of this degradation-related defect [2]. Such defect characterization could benefit from applying deep-level transient spectroscopy (DLTS), which is a capacitance-based technique for detecting and quantifying defect levels due to impurities and/or crystal imperfections that may capture carriers, increase carrier recombination, and lead to reduced solar cell performance [3]–[5]. DLTS can measure a defect state's activation energy, trap density, and capture cross section for the capture of minority or majority carriers. Previous work has applied DLTS to identify the defect state in LeTID-affected multicrystalline silicon cells [6], [7]. Minority-carrier traps of E_C-0.19 eV and E_C-0.34 eV for LeTID in multicrystalline cells have been reported [6]. Majority-carrier traps possibly involving an interstitial iron defect or complex with activation energies of 0.295 and 0.485 eV have also been reported [7]. We have previously presented DLTS data on a LeTID-related defect found in monocrystalline silicon solar cells [8]. Here, we build upon those initial results by additionally comparing DLTS measurements on the same sample before and after regeneration, comparing long and short filling pulsewidths, and directly measuring the defect capture rate.

II. Experiment

We have selected monocrystalline-silicon fielded modules from a utility-scale installation where some modules had shown relatively reduced performance after about three years [9]. One of these lower performance modules is stressed with current (short-circuit current−maximum power current) at 75 °C for two weeks. This process is an accelerated degradation stress for LeTID. No additional degradation is observed, which suggests that the modules fully degraded by LeTID in the field. The module is then processed using an accelerated regeneration phase, which includes three weeks of short-circuit current at
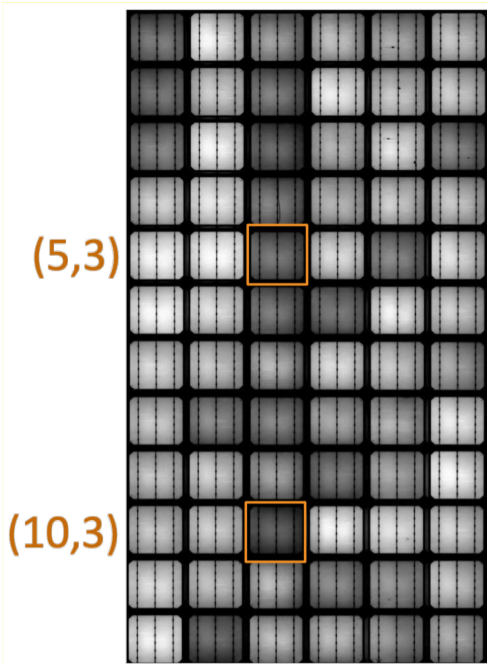
Fig. 1. PL images of the cells within the LeTID-degraded module. Squares are drawn around two of the darker cells. These selected cells are cored to obtain cell fragments for testing.
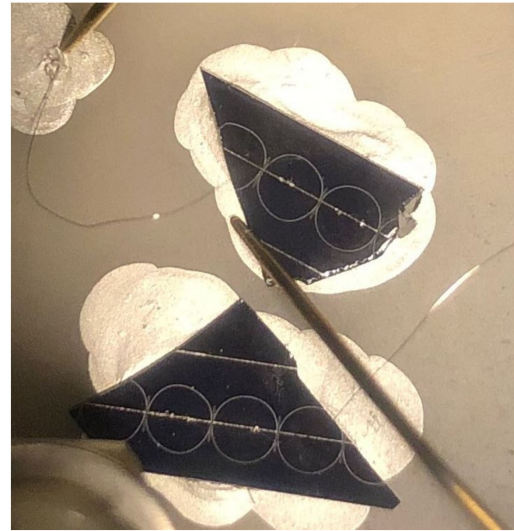

Fig. 2. Cell fragments are mounted in the DLTS cryostat using silver paint. Laser micromachining is used to isolate 1-mm radius areas around grid lines. Wire bonding and probes make contact to the isolated device areas.

85 °C. The module reverses its power degradation and increases power by approximately 2%. Photoluminescence (PL) and electroluminescence (EL) imaging show that some cells within the module change more than others, and this cell-to-cell variation is also a trait of LeTID. On a second module that is in the as-received condition from the field, PL imaging similarly shows that some cells within the module had degraded more than others. Based on the results of the first module, we choose cells from the second module that are relatively dark in PL counts since these dark cells would be examples of the highest effect of LeTID and largest improvements during regeneration. The PL images of the cells within the module and the cells chosen for coring out cell fragments are shown in Fig. 1.

Cores are extracted from the highlighted cells [(5,3) and (10,3)] of Fig. 1 using a drill and 20-mm-diameter diamond coring bit as similarly described in [10]. During the coring process, the backsheet is initially removed using a depth-controlled router and peeling of remaining encapsulation layers by hand. A metal stub is glued to the back of the solar cell, and a hole saw is used to cut the cell around the stub. The stub with glued cell is then removed using a wrench, and the glue is dissolved by soaking the stub and cell piece in acetone. No significant heating is detected, as the stub remains cool to touch during cutting. The hole saw cuts at the outer perimeter of the cell piece, and no significant contamination source is expected due to the cutting and immersion in acetone.

Our measurements include four DLTS experiments to be discussed in the following order.

1) Comparison of a LeTID degraded sample to a separately regenerated sample, both from (5,3).

2) Regeneration of the degraded sample and comparison to its degraded state.
3) Comparison of the same degraded and regenerated sample using a longer filling pulse time.
4) Repeating the degraded-state measurement on a different cell (10,3) along with direct measurement of the defect's capture rate.

The capacitance meter for the DLTS system requires a capacitance smaller than 3000 pF. For typical solar cell doping values, this capacitance corresponds to a sample size in the millimeter range. Some cores cracked during removal from the module or were intentionally cleaved when only smaller areas were needed. We have taken fragments of the cored cell pieces and used a femtosecond ultra-short-pulse laser to micromachine a circle pattern through the top layers of the cell [11]. There are separate cuts to initially cut through the metal grid finger at the edges of the circles. Then, there are shallow circle cuts ($\sim$10-μm deep) to define 1-mm radius circles to isolate and define a small-area device. The sample is mounted on a thin, electrically insulating, thermally conductive AlN substrate using silver paint, as shown in Fig. 2. The silver paint is oversized so that the back contact can be probed. The silver paint also provides thermal conductivity between the sample and substrate. A wire bonder is used to connect the narrow grid finger to a larger silver paint spot. This helps to make a consistent top contact for the probe in the cryostat due to some movement from thermal contraction and expansion. A separate temperature sensor (not shown) is pinned to the top of the sample for measuring sample temperature during temperature sweeps.

Throughout the temperature sweeps used for DLTS data collection, current-voltage and capacitance-voltage data are collected roughly every 10 °C to measure the reverse leakage current and carrier concentration. For both conditions of LeTID-degraded and regenerated, several measurements of samples from cell (5,3) are shown in Fig. 3. When starting the temperature
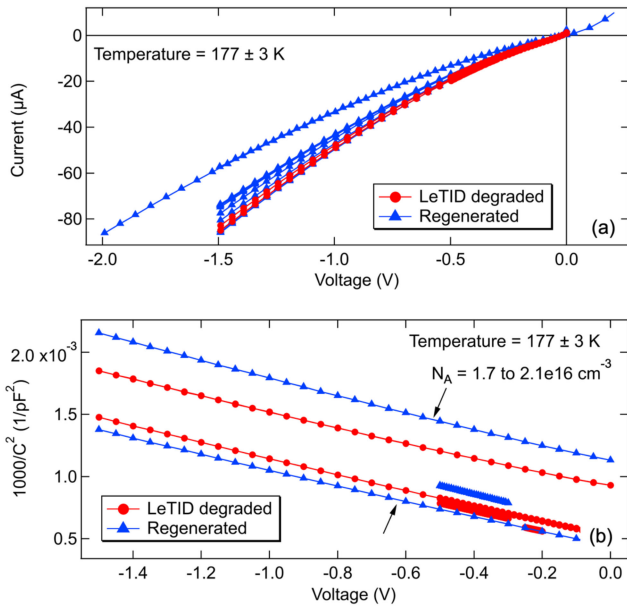
Fig. 3. For several DLTS measurements, (a) current-voltage sweeps and (b) capacitance-voltage sweeps for temperatures of 177 ± 3 K are plotted. Versions of samples are represented by red circles for LeTID-degraded and blue triangles for regenerated samples. The slope of the $1/C^2$ versus bias plot corresponds to the carrier concentration, or doping, which varies between 1.7×10^{16} to 2.1×10^{16} cm^{-3} at the temperature range where DLTS peaks are observed.

Fig. 4. Capacitance transient amplitudes are extracted using Fourier transforms, and these values for the 10-ms time window are plotted as a function of temperature. The peak value corresponds to a trap density of 1.1×10^{13} cm^{-3} for the LeTID-degraded sample and 2.1×10^{12} cm^{-3} for the separate regenerated sample.

Fig. 5. DLTS data from analyzed time windows are graphed in an Arrhenius plot. The majority-carrier hole traps have an activation energy of 0.42 ± 0.02 eV. Capture cross sections are calculated based on the y-intercept values of the fits and range from 2.5×10^{-13} to 5.2×10^{-13} cm^2.

sweep at a lower temperature, a larger reverse bias can be applied without exceeding leakage current in the range of hundreds of microamperes. This is to prevent overloading the capacitance meter and possibly degrading the transient response. As shown in Fig. 3(a), reverse current values at temperatures near 177 K remain smaller than 100 μA for bias values of -1.5 to -2.0 V.

Using the 1-mm radius area and a relative dielectric constant value of 11.9 for silicon, the p-type carrier concentration is calculated at temperatures near 177 K. For both LeTID-degraded and regenerated samples, the doping values are between 1.7×10^{16} and 2.1×10^{16} cm^{-3}, as shown in Fig. 3(b). Variations in laser scribing, probing condition, and spatial cell doping may lead to small changes in calculated doping, but no trend or significant differences are seen when comparing LeTID-degraded to regenerated versions of the samples.

A. DLTS on Separate Samples

The first DLTS experiment uses two separate cores cut from cell (5,3) where one is kept in its degraded state, whereas another is subjected to the regeneration procedure of applying rated short-circuit current for that sample's area for two weeks at 85 °C. We use a PhysTech (formerly Bio-Rad and Accent Optical Technologies) DLTS system based on fast Fourier transforms of the capacitance transients [5]. DLTS data are collected using 12 transient-analysis time windows from 5 ms to 20 s for temperature sweeps between room temperature, or slightly lower, and roughly 50 K. Each transient is averaged for 3 min to improve the signal-to-noise ratio. For both samples, the applied bias is -0.5 V (reverse), and the filling pulse is 50 μs in length at a bias of 0.25 V (forward). The DLTS signals for the 10-ms time windows are
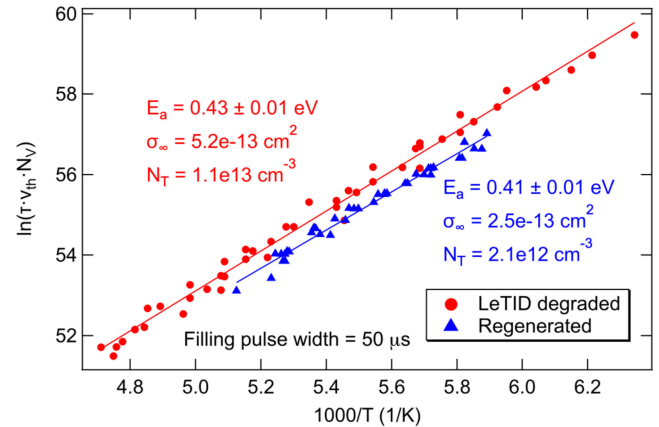
shown in Fig. 4. For this time window, both the LeTID-degraded and regenerated samples show a negative peak near 190 K. A negative peak corresponds to trapping and emission of majority carriers, or holes in this case of a p-type base solar cell. Based on the peak amplitudes and the doping values, the defect trap concentration, N_T, can be estimated as 1.1×10^{13} cm^{-3} for the LeTID-degraded sample and 2.1×10^{12} cm^{-3} for the separately regenerated sample. The regenerated sample shows a similar peak position, and the smaller signal corresponds to a decrease in the defect trap concentration by about a factor of five.

The DLTS data from the measured time windows are fit to match the time constants to the corresponding peak temperatures. These data are plotted in the Arrhenius summary graph in Fig. 5. The similar slope values for both the LeTID-degraded and regenerated samples correspond to a hole-trap activation energy with respect to the valence band of 0.42 ± 0.02 eV. There are fewer data points for the regenerated sample due to the weaker signal and relatively higher noise level that prevents
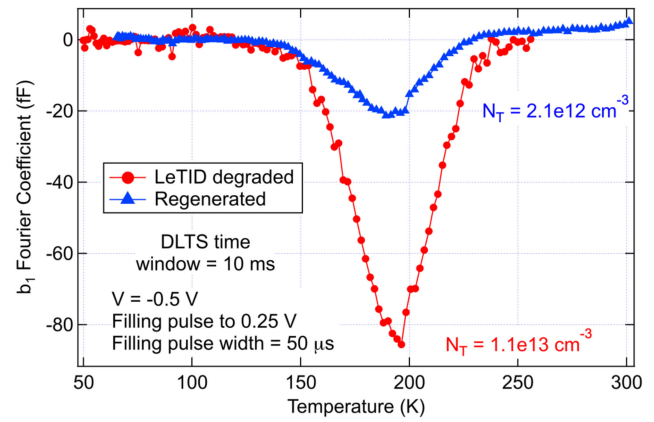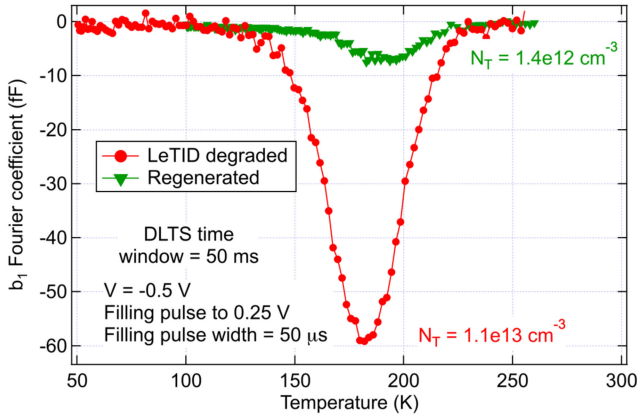
Fig. 6. Capacitance transient amplitudes are extracted using Fourier transforms, and these values for the 50-ms time window are plotted as a function of temperature. The peak value corresponds to a trap density of 1.1×10^{13} cm^{-3} for the sample's LeTID-degraded state and 1.4×10^{12} cm^{-3} after the sample has been regenerated.
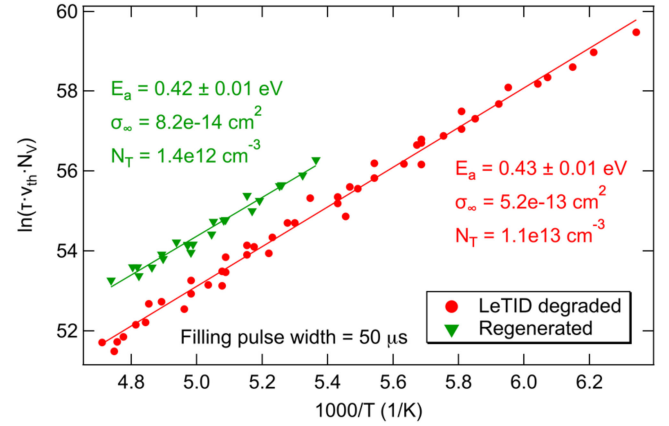

Fig. 7. DLTS data from analyzed time windows are graphed in an Arrhenius plot. The majority-carrier hole traps have an activation energy of 0.42 ± 0.02 eV. Capture cross sections are calculated based on the y-intercept values of the fits and range from 8.2×10^{-14} to 5.2×10^{-13} cm^2.

accurate fitting of peaks. The corresponding y-intercept capture cross sections are calculated using a silicon hole effective mass (density of states) of $0.56m_o$ (default value from the silicon library of parameters within the PhysTech software), where m_o is the electron mass. These values of apparent capture cross section σ_∞ range from 2.5×10^{-13} to 5.2×10^{-13} cm^2, and represent a defect fingerprint based on the data in the Arrhenius plot. These values may not represent the true capture rate at room temperature. In our last presented experiment below, we measure the capture rate directly at temperatures where DLTS peaks occur.

B. DLTS on Same Regenerated Sample

In our second experiment, we use the degraded sample of the first experiment and apply a regeneration procedure. The area of the laser-scribed device is 3.14 mm^2, and the area-rated short-circuit current is roughly 1.2 mA. To perform the regeneration process, a forward-bias voltage is applied to maintain this current while the sample is kept at 85 °C for two weeks. The sample is then measured by DLTS using the same conditions, which are applied bias of –0.5 V, filling pulse to 0.25 V, and filling pulsewidth of 50 μs. The DLTS data for the 50-ms time window are plotted in Fig. 6. For this slightly longer time window, the peaks shift to a colder temperature near 180 K, and the signal amplitude is slightly lower. The reduced amplitude is possibly due to more noise in the data since fewer transients are averaged in the 3-min acquisition time when compared to the shorter time windows of 5 or 10 ms, or the capacitance decay signal may be somewhat nonexponential. Many time windows and Fourier coefficients are used during the peak fitting process, so the trap density values are averages of up to 100 amplitude fits. As similarly seen in Section II-A, the defect concentration is reduced due to the applied regeneration procedure. For this before-and-after measurement of the same sample, the trap density has decreased from 1.1×10^{13} to 1.4×10^{12} cm^{-3}, which is nearly a factor of

eight reduction, compared to the factor of five for the separate pieces presented in Section II-A.

The peak temperature values for the range of time windows are similarly plotted on an Arrhenius plot. These data shown in Fig. 7 give similar activation energies of 0.42 ± 0.02 eV for the defect level for both before and after regeneration. The capture cross section σ_∞ values of 8.2×10^{-14} and 5.2×10^{-13} cm^2 are also very similar, as the Arrhenius plot data for before and after regeneration are nearly colinear.

C. DLTS on Same Sample With Longer Filling Pulse

In the third experiment, we compare the sample of the second experiment where DLTS is measured on the same sample before and after the regeneration treatment. In the second experiment, we used a short filling pulsewidth of 50 μs, which is just above the manufacturer's recommendation for pulsewidth resolution (20 μs) when using the built-in pulse generator. Here, we measure the intensity of the DLTS signal as a function of filling pulsewidth. The sample is kept at a constant temperature of 200 K, where a suitable length of time for the defect's emission rate is 10 to 20 ms. The sample is biased at –1.5 V, whereas pulses to 0 V are used to move the edge of the depletion region and fill empty defect states with holes. Filling pulses of increasing width are used to monitor the capture of holes by the defects. Linear steps are used for the shortest filling times (1 to 50 μs), whereas a second measurement using logarithmic steps extends filling pulsewidths out to 20 ms. As shown in Fig. 8, trap states mostly fill before reaching the resolution of the built-in pulse generator. However, the transient amplitudes continue to increase with increasing filling pulsewidths, even out to 20 ms. Also, for silicon, similar profiles of the increasing DLTS signal amplitude with longer filling pulse times have been observed and attributed to extended defects, such as dislocations or defect clusters [12].

The DLTS data for before and after regeneration when using a 20-ms filling pulsewidth are shown in Fig. 9. The time window of 200 ms has a peak around 175 to 180 K. The LeTID-degraded state corresponds to a trap density of 1.4×10^{13} cm^{-3}, whereas
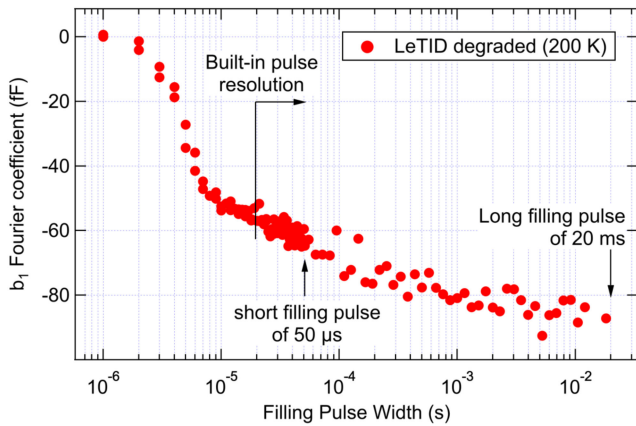
Fig. 8. Capacitance transient amplitudes are plotted as a function of filling pulsewidth for a LeTID-degraded sample. Data points using filling pulsewidths less than 20 μs are not accurate due to resolution limitations of the built-in pulse generator.

Fig. 10. DLTS data from analyzed time windows are graphed in an Arrhenius plot. A longer filling pulsewidth of 20 ms has been used. The majority-carrier-hole traps have an activation energy of 0.36 ± 0.02 eV. Capture cross sections are calculated based on the y-intercept values of the fits and range from 3.2×10^{-15} to 8.0×10^{-15} cm^2.
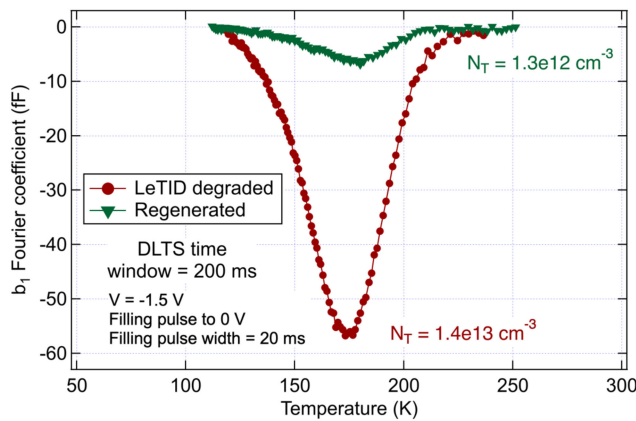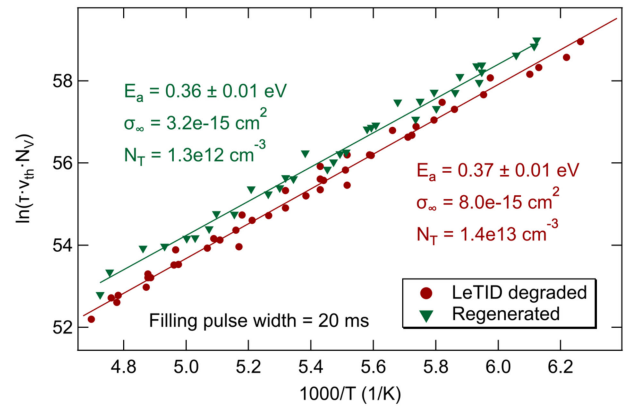

Fig. 9. Capacitance transient amplitudes are extracted using Fourier transforms, and these values for the 200-ms time window are plotted as a function of temperature. A longer filling pulsewidth of 20 ms has been used. The peak value corresponds to a trap density of 1.4×10^{13} cm^{-3} for the sample's LeTID-degraded state and 1.3×10^{12} cm^{-3} after the sample has been regenerated.
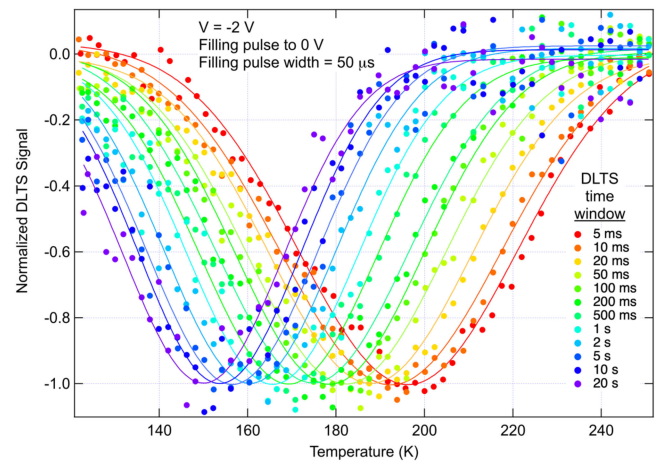

Fig. 11. Amplitudes of capacitance transients are extracted using Fourier transforms, and these values for all of the time windows are normalized for clarity and plotted as a function of temperature. Gaussian fits are shown as solid lines.

the same sample after regeneration gives a reduced density of 1.3×10^{12} cm^{-3}. This is near a factor of ten decrease in active defect concentration. The data from other time windows and corresponding temperature peaks are plotted in the Arrhenius plot of Fig. 10. The fits of these data now show that the activation energy is slightly lower with values of 0.36 to 0.37 eV. The longer filling pulses have continued to fill defect states, and the smaller activation energy for long filling pulse times suggests that the defects may consist of a band of states. Deeper states fill first with short pulsewidths, but as the filling times become longer and the defect states tend toward saturation, possible tails of states nearer to the valence band become filled. These states would then emit with a lower activation energy, as measured here. Others have shown DLTS peak broadening and peak shift to lower temperature when the filling pulse is lengthened, and these effects have been observed for extended defects, such as clusters, precipitates, platelets, and impurity-decorated dislocations, which have a degree of bandlike states as opposed to localized states [13]–[15].

D. Other Cell, Direct Capture Measurement

In the fourth experiment, we use a cored piece from cell (10,3) to show repeatability of detecting the defect level and also for directly measuring the capture rate of holes in this LeTID-degraded state of the defect. The (10,3) core is similarly prepared for DLTS by laser micromachining a 1-mm-radius isolated area. A bias of -2 V is applied to the sample with a filling pulse to 0 V having a pulsewidth of 50 μs. All 12 time windows from 5 ms to 20 s are used, and the results are shown in Fig. 11. The DLTS signals for all time windows are normalized and fit with Gaussian functions to show the temperature shifts and peak widths with better clarity. The peak amplitudes decrease with longer time windows as seen in Figs. 4 and 6, and this is possibly due to nonexponential decay shapes or weaker and noisier signals when fewer transients are averaged for the longer time periods. Nonexponential behavior of the capacitance transient may be attributed to the broadened defect
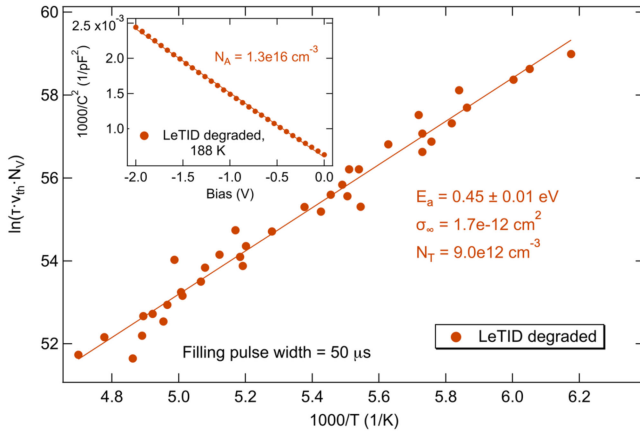
Fig. 12. DLTS data from analyzed time windows are graphed in an Arrhenius plot. The majority-carrier hole traps have an activation energy of 0.45 ± 0.01 eV. The apparent capture cross section is calculated based on the y-intercept value of the fit and is given as 1.7×10^{-12} cm^2. The inset graph shows a capacitance-voltage sweep for 188 K, which is within the range of temperatures where DLTS peaks occur. The slope of the $1/C^2$ versus bias plot corresponds to the doping and gives a value of 1.3×10^{16} cm^{-3}.

band or electric-field dependence of the emission of holes in the depletion region [3].

The peak temperature values for the corresponding time window values from Fig. 11 are graphed in an Arrhenius-plot format in Fig. 12. The trap values for this sample from cell (10,3) are fit from the Arrhenius plot to give an activation energy of 0.45 eV and a capture cross section of 1.7×10^{-12} cm^2. The amplitudes of the capacitance transients give a trap concentration of 9.0 $\times 10^{12}$ cm^{-3}. The hole concentration at 188 K is fit from the capacitance-voltage sweep, as shown in the inset of Fig. 12, to give a value of 1.3×10^{16} cm^{-3}. These values are very similar to those measured on the cell (5,3) sample ($N_T = 1.1 \times 10^{13}$ cm^{-3} from Fig. 6, $E_a = 0.43$ eV from Fig. 7, and $N_A = 2.0 \times 10^{16}$ cm^{-3} from Fig. 3) when using the same filling pulsewidth of 50 μs. This sample is then further characterized in its LeTID-degraded state and is not regenerated.

The apparent capture cross-sectional values σ_∞ have been calculated from the Arrhenius plots based on the y-intercept value of the linear fit along with thermal velocity and density of states. These terms include Boltzmann's constant, Planck's constant, and silicon's effective mass for holes, in this case. But, as noted before, σ_∞ may not represent an actual capture rate at room temperature. As previously shown in Fig. 8, the DLTS signal amplitude can be used to monitor the captured number of holes in the previously empty defect states. The built-in signal generator is not fast enough to accurately measure the initial capture rate of holes, and our PhysTech system does not have a fast pulse interface option. We use an HP 8112A signal generator that is capable of producing pulses with nanosecond time resolution. The pulses have well-behaved rise and fall transients when the signal is terminated into the low impedance of an oscilloscope, but unknown transient effects may be present when the pulses are terminated into the capacitive impedance of the sample. The coaxial cables are kept as short as possible ($\sim$30 cm), but transient effects may distort the pulse and lead to
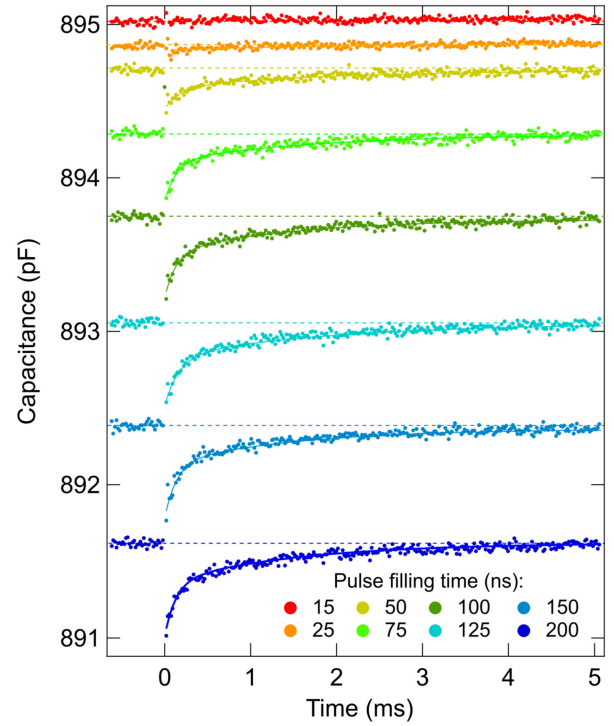

Fig. 13. DLTS transients are captured as a function of filling pulsewidth. The sample is held at –2 V with filling pulses to 0 V of time widths of 15 to 200 ns. The curves are offset in the y-axis for clarity. The transient data are represented by dots, whereas an exponential fit is shown by a solid line.

uncertainty in the shape and effective width of the actual voltage pulse. The pulse generator uses a 10-ms period, and pulses can be applied with widths of 10 ns and longer.

We have collected capacitance transients using a Zurich Instruments MFIA impedance analyzer. The MFIA receives a trigger signal from the pulse generator at the same time the sample is pulsed with a filling voltage pulse from -2 to 0 V and back to -2 V again. The MFIA is set to average up to 50 000 pulses ($\sim$50 min) for improving the signal-to-noise ratio and being able to resolve down to 10-fF values out of a sample baseline capacitance of almost 1000 pF, which corresponds to a sensitivity of roughly 1 part per 10^5. At a sample temperature of 205 K, the defect's emission rate gives a capacitance transient that decays on the order of a few milliseconds. As shown in Fig. 13, the amplitude of the capacitance transient increases as the filling pulsewidth is increased.

The curves are offset in the y-axis for clarity, where the dashed line shows the offset baseline value for each transient. The data are represented as dots in the graph, and exponential fits are shown as solid lines. The sample temperature is also decreased to 190 K and increased to 220 K, and similar data are collected. The transient amplitude values are taken from the fits, and these are used to calculate a capture rate for the defect. A fraction of empty traps $F(t_f)$ is defined as follows [3]:

$$F(t_f) = 1 - n_t(t_f) / n_t(\infty) \tag{1}$$

where $n_t(\infty)$ is the steady-state value of filled traps when the filling time t_f is large, or 50 μs in this case. Equation (2) relates
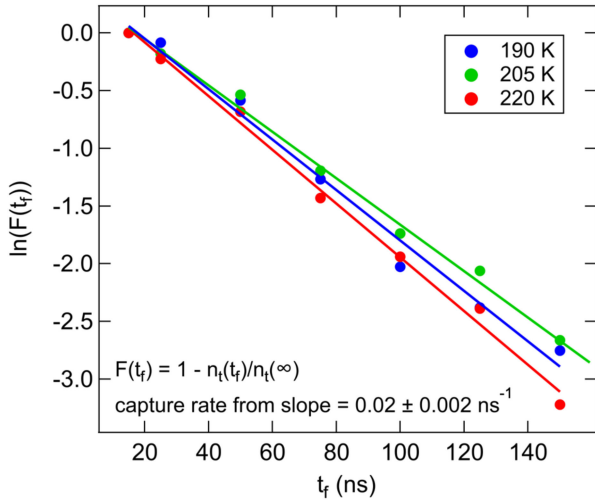
Fig. 14. Capture rate of holes in the defect is measured using increasing filling pulsewidths from 15 to 150 ns at temperatures of 190, 205, and 220 K. $F(t_f)$ represents the fraction of empty traps, and the natural log scale encompasses the range of all traps being empty to ~95% of traps being filled.

this fraction of empty traps to the time-dependent capture and emission [3]

$$F(t_f) = \exp\left[-(e_p+c_p)\,t_f\right] \qquad (2)$$

where e_p is the emission rate of holes from the trap, and c_p is the capture rate. The analysis applies to initial capture of holes when the hole-occupied number of traps is small compared to the total trap density, and when the total trap density is much lower than the doping, as it is in this case for ~10^{13} cm^{-3} traps in ~10^{16} cm^{-3} doping. Here, the emission is on the order of milliseconds, whereas the capture is occurring in the first 100 ns, so the emission rate is negligibly small. As shown in Fig. 14, $\ln(F(t_f))$ is plotted as a function of t_f for the three temperatures (190, 205, and 220 K). The slope corresponds to the capture rate, and linear fits to the logarithmic data give a value of 0.022 ± 0.002 ns^{-1}.

The capture rate data do not show a clear trend with temperature, so we make the assumption to use this capture rate at room temperature. The capture rate c_p is also defined [3] as follows:

$$c_p = p\sigma_p v_{\text{th}} \qquad (3)$$

where p is hole density, σ_p is the hole capture cross section, and v_{th} is the thermal velocity. Using an effective mass (conductivity) for holes of $0.36m_{\text{o}}$ and a hole doping value of 2.2×10^{16} cm^{-3}, the hole capture cross section for this defect is 5.1×10^{-17} cm^2 at 300 K. This directly measured value is smaller than σ_∞ from the Arrhenius plots' intercept values that ranged from ~10^{-15} to 10^{-12} cm^2. The majority-carrier-hole lifetime τ_p due to this defect level is calculated using the following [3]:

$$\tau_p = 1/N_T \sigma_p v_{\text{th}}. \qquad (4)$$

For values of $N_T = 1 \times 10^{13}$ cm^{-3}, $\sigma_{\text{p}} = 5 \times 10^{-17}$ cm^2, and $T = 300$ K, the defect's majority-carrier-hole lifetime is around 100 μs. This lifetime value contributes to the overall effective lifetime of the solar cell device when it is operating

with an excess carrier density near the doping value of ~10^{16} cm^{-3} or higher. Excess carrier lifetime is often not a single value when considering variations in carrier concentration. For a nonradiative defect center near the mid-gap, the recombination rate depends mostly on capture of minority carriers at low injection (below the doping level) and the capture rate of both carriers at higher injection.

When the solar cell device is regenerated, and the trap density N_T is reduced by roughly a factor of ten, then the defect-related majority-carrier-hole lifetime is increased to ~ 1 ms. The defect lifetime contributes to carrier recombination in parallel to other intrinsic and defect- or interface-related recombination mechanisms. Assuming that intrinsic recombination mechanisms, such as radiative and Auger, are negligible, the defect's lifetime, estimated here to be ~100 μs, can be significant and lead to reduced cell performance at concentrations found in the LeTID-degraded state. When regenerated, the lifetime increases by an amount proportional to the decrease in active defect concentration. Here, we have measured three cases where N_T decreases by factors of five to ten when the samples were regenerated. Others have observed carrier lifetime degradation near factors of four [16], five [17], and ten [18] at high-temperature firing conditions for LeTID-affected monocrystalline p-type silicon. These lifetime values are evaluated at injection levels of ~1 to 5×10^{15} cm^{-3}, which is within an order of magnitude below the doping level and where capture of majority-carrier holes may influence the effective lifetime. The injection level regime of these lifetime results may be approaching the conditions where the DLTS defect level measured here can influence carrier recombination. Nevertheless, the change in N_T observed here by DLTS gives results that are similar to reported changing carrier lifetime values when LeTID transitions from the degraded to the regenerated state.

III. CONCLUSION

Monocrystalline silicon modules have been acquired from a utility-scale field after showing relatively lower performance after three years. Based on a regeneration process, the modules are determined to have degraded by LeTID. Cored cell fragments from cells within one of the degraded modules are extracted. We show repeatable DLTS results, which reveal a hole trap with an activation energy of ~0.42 eV. The trap concentration is reduced from ~10^{13} to ~10^{12} cm^{-3} when a regeneration process is applied. Long filling pulses lead to a slight reduction of activation energy to 0.37 eV, which suggests the defect possesses some tail states that extend toward the valence band. Direct measurement of the capture rate gives a capture cross section of 5×10^{-17} cm^2 for this defect. Considering the defect concentration, the defect-related majority-carrier lifetime would be ~100 μs when in the LeTID-degraded state, but then increase to ~1 ms upon regeneration.

REFERENCES

[1] K. Ramspeck *et al.*, "Light induced degradation of rear passivated mc-Si solar cell," in *Proc. 27th Eur. Photovolt. Sol. Energy Conf. Exhib.*, 2012, pp. 861–865.

[2] D. Chen *et al.*, "Progress in the understanding of light- and elevated temperature-induced degradation in silicon solar cells: A review," *Prog. Photovolt. Res. Appl.*, vol. 29, no. 11, pp. 1180–1201, Nov. 2020.

[3] P. Blood and J. W. Orton, *The Electrical Characterization of Semiconductors: Majority Carriers and Electron States*. San Diego, CA, USA: Academic, 1992.

[4] D. K. Schroder, "Defects," in *Semiconductor Material and Device Characterization*, 3rd ed. Hoboken, NJ, USA: Wiley, 2006, pp. 251–317.

[5] S. Weiss and R. Kassing, "Deep level transient Fourier spectroscopy (DLTFS)—A technique for the analysis of deep level properties," *Solid-State Electron.*, vol. 31, no. 12, pp. 1733–1742, 1988.

[6] T. Mchedlidze and J. Weber, "Location and properties of carrier traps in mc-Si solar cells subjected to degradation at elevated temperatures," *Physica Status Solidi A, Appl. Mater. Sci.*, vol. 216, no. 17, 2019, Art. no. 1900142.

[7] Z. Chunlan, Z. Su, J. Fangxu, and W. Wenjing, "Deep level transient spectroscopic investigation of carrier trap defects in p-type mc-Si PERC solar cells after elevated temperature light soaking," in *Proc. 36th Eur. Photovolt. Sol. Energy Conf. Exhib.*, 2019, pp. 147–150.

[8] S. Johnston *et al.*, "LeTID-affected cells from a utility-scale photovoltaic system characterized by deep level transient spectroscopy," in *Proc. IEEE 48th Photovolt. Specialists Conf.*, Jun. 2021, pp. 2276–2278.

[9] M. G. Deceglie *et al.*, "Light and elevated temperature induced degradation (LeTID) in a utility-scale photovoltaic system," *IEEE J. Photovolt.*, vol. 10, no. 4, pp. 1084–1092, Jul. 2020.

[10] H. R. Moutinho *et al.*, "Development of coring procedures applied to Si, CdTe, and CIGS solar panels," *Sol. Energy*, vol. 161, pp. 235–241, 2018.

[11] S. Johnston, D. B. Sulas, and G. F. Kroeger, "Laser cutting and micromachining for localized and targeted solar cell characterization," in *Proc. 46th IEEE Photovolt. Specialists Conf.*, Jun. 2019, pp. 2753–2757.

[12] C. Wang, M. Zhao, W. Li, and E. Simoen, "Impact of in situ annealing on the deep levels in Ni-Au/AlN/Si metal-insulator-semiconductor capacitors," *Phys. Status Solidi A*, vol. 216, no. 16, 2019, Art. no. 1900248.

[13] F. Riedel and W. Schroter, "Electrical and structural properties of nanoscale $NiSi_2$ precipitates in silicon," *Phys. Rev. B*, vol. 62, no. 11, pp. 7150–7156, 2000.

[14] M. Seibt, R. Khalil, V. Kveder, and W. Schroter, "Electronic states at dislocations and metal silicide precipitates in crystalline silicon and their role in solar cell materials," *Appl. Phys. A*, vol. 96, no. 1, pp. 235–253, 2009.

[15] H. Hedemann and W. Schroter, "Deep-level transient-spectroscopy for localized states at extended defects in semiconductors," *J. Phys. III*, vol. 7, no. 7, pp. 1389–1398, Jul. 1997.

[16] D. Lin *et al.*, "New insights on LeTID/BO-LID in p-type mono-crystalline silicon," *Sol. Energy Mater. Sol. Cells*, vol. 226, Jul. 2021, Art. no. 111085.

[17] D. Chen *et al.*, "Evidence of an identical firing-activated carrier-induced defect in monocrystalline and multicrystalline silicon," *Sol. Energy Mater. Sol. Cells*, vol. 172, pp. 293–300, Dec. 2017.

[18] T. Niewelt *et al.*, "Light-induced activation and deactivation of bulk defects in boron-doped float-zone silicon," *J. Appl. Phys.*, vol. 121, no. 18, May 2017, Art. no. 185702.